2014

High Definition Sounding System (HDSS) for atmospheric profiling

Black, Peter

High Definition Sounding System (HDSS) for atmospheric profiling

Peter Black[1], Lee Harrison[2], Mark Beaubien[3], William Jeffries[3], Robert Bluth[4], Haflidi Jonsson[4], Andrew Penny[5] and Robert W. Smith[6]

[1]Naval Research Laboratory
Marine Meteorology Division
SAIC, Inc
Surveillance and Reconnaissance Solutions Division
[2]University at Albany, State University of New York Atmospheric Sciences Research Center
Albany, NY
[3]Yankee Environmental Systems, Inc.
[4]Naval Postgraduate School
Center for Interdisciplinary Remotely Piloted Aircraft Studies
[5]Naval Postgraduate School
Meteorology and Physical Oceanography Department
[6]NASA/ Johnson Space Center
WB-57 Program Office, Ellington Field

Introduction

Widely-used Tropical Cyclone (TC) models include regional air-sea coupled dynamical models such as COAMPS-TC (Hao, et al, 2013), HWRF (Tallapragada, et al., 2014; Kim, et al., 2014) and GFDL (Bender et al., 2007; Gall, et al., 2011), global dynamical models such as GFS and ECMWF, and statistical-dynamical intensity-prediction models such as SHIPS, STIPS, L-GEM, RII (DeMaria and Kaplan, 1999; DeMaria, et al., 2005; Knaff et al., 2005; Jones, et al., 2006; DeMaria, 2009; DeMaria, 2010; Kaplan, et al., 2010). All of these models benefit from improved 3-D spatial observational plus enhanced temporal resolution, i.e. better 4-D capability. The need for enhanced 4-D profile observations is driven by the need for enhanced model resolution of the physics of small-scale processes such as convective events, boundary layer air-sea transfer processes and upper troposphere outflow jets. These requirements demand a concurrent enhancement in 4-D profile observational capability at finer spatial and temporal scales. Observations and observational strategies for initial condition specification and forecast validation within and around TCs require continual improvement to match these model demands while providing a basis for improvements in process understanding and parameterization on increasingly smaller scales.

The advent of *in-situ* dropsonde atmospheric profiling (Hock and Franklin, 1999; Franklin, et al., 2003) has played a key role in contributing to this need and demonstrating improved model track prediction performance (Burpee et al., 1996; Aberson and Franklin, 1999; Weissman, et al., 2011; Aberson, 2011; Kun-Hsuan, et al., 2011; Wu, et al., 2007). The use of dropsonde observations has also become the 'reference standard' by which enumerable satellite and airborne remote sensors have been validated. These advances have, in turn, resulted in TC track improvements (Uhlhorn et al, 2003; Uhlhorn et al, 2007). Use of 3D winds from TC airborne Doppler radar observations in numerical prediction models such as WRF-ARW using an Ensemble Kalman Filtering (EnKF) scheme (Weng and Zhang, 2012) have also shown promise.

However, despite advanced observational technology and model advancement, there has been little improvement in official predictions of TC intensity, either in the Atlantic or Pacific basins (DeMaria, et al, 2014).

The HDSS has been developed by Yankee Environmental Systems, Inc. (YES, Inc.) to meet the needs of Naval Research Laboratory field programs. The HDSS consists of eXpendable Digital Dropsondes (XDDs), and the Automated Dropsonde Dispensers (ADD). The design allows rapid-deployment, multi-sonde sampling strategies over the TC inner core as well as detailed observation of TC outflow and inflow layer mesoscale features. The goal is to improve understanding and prediction of TC intensity, especially Rapid Intensification (RI) and Rapid Decay (RD) events.

A predecessor of the XDD known as the XDR was demonstrated on the NASA DC-8 during the Arctic Mechanisms of Interaction between the Surface and Atmosphere (AMISA 2008) project in which 36 XDRs were deployed over 6 days, including several showing excellent intercomparisons with radiosonde ascents from the Swedish icebreaker Oden (Gasiewski, 2009; Persson, 2010).

The HDSS has been validated during a series of collaborative test flights with 1) Naval Postgraduate School, Center for Interdisciplinary Remotely-Piloted Aircraft Studies (CIRPAS), using their Twin Otter aircraft, 2) NASA Wallops Flight Facility (WFF), using their P-3 aircraft, 3) NASA Dryden Flight Research Center (DFRC), using their DC-8 Airborne Science Laboratory, and 4) NASA Johnson Space Center- Ellington Field (JSC-EF), using their WB-57 aircraft. Results presented are based on two Twin Otter flights with XDD deployments from 4 km altitude, one DC-8 flight with XDDs deployed from 12 km altitude and three WB-57 flights with deployments from 18 km altitude. These tests were conducted, respectively, 1) from the CIRPAS facility in Marina, CA over National Data Buoy Center (NDBC) buoys off shore from the California coast, 2) from DFRC at Edwards, CA over the Eastern Pacific east of TC Cosme and southwest of Cabo San Lucas, Mexico and 3) from JSC-Ellington Field, TX over the western Gulf of Mexico offshore from the Texas coast adjacent to NWS radiosonde stations at Brownsville (BRO) and Corpus Christi (CRP) and NDBC buoys.

The objectives achieved from each of these flights were, respectively: 1) successful demonstration in 2011 of observational repeatability (same profile measurements from repeated deployments in similar environments) as well as good agreement between XDD profile observations and concurrent and collocated independent observations, 2) successful demonstration and certification in 2012 of ADD launch capability in pressurized aircraft, 3) successful demonstration in 2013 of high-speed (240 m/s TAS), high-altitude (12 km) XDD deployments and data recovery from extreme range (120 km) using fast- and slow-fall modes of descent and 4) successful approval for flight from Technical Readiness Review in 2013, successful demonstration of HDSS transition from prototype to the operational Mark B, successful demonstration of moderate-speed (120 m/s TAS), extreme altitude (20 km) XDD deployments, data recovery from extreme ranges (160 km) and good agreement between XDD profile observations and concurrent, near environment independent observations. In the following sections the HDSS technology is described as well as each of the three aircraft flight experiments. The extent of this effort requires supplementary material; some figures and

associated notes therein are referenced here as "S."

XDD/HDSS Description

The XDD measures GPS location and altitude and vertical profiles of Pressure, Temperature, hUmidity (PTU), horizontal and vertical velocity (horizontal velocities are taken to be the wind), as well as Sea Surface Temperature (SST). The XDD weighs 58 g and is 17.8 cm long and 6.6 cm in diameter. Sondes are activated and programmed before launch via a non-contact optical interface to select communication parameters prior to release. The XDD board layout with component parts labeled and current packaging is shown in figure 1.

The XDD contains no parachute and its center of gravity can be adjusted to select either a ballistic fast-fall or spiral-dive slow-fall mode of descent. Sea-level descent rates are approximately 18 m/s for the fast-fall and 10 m/s for the slow; the latter is more variable. Descent time from 18 km to the surface is approximately 11 minutes for the fast and 17-18 minutes for the latter. All sondes deployed at CIRPAS were slow-fall sondes, with the goal of matching RD-94 descent rates; this turned out to be disadvantageous for the XDDs, as will be shown. While subsequent test flights deployed both modes we expect further use to primarily be fast-mode, for reasons shown later.

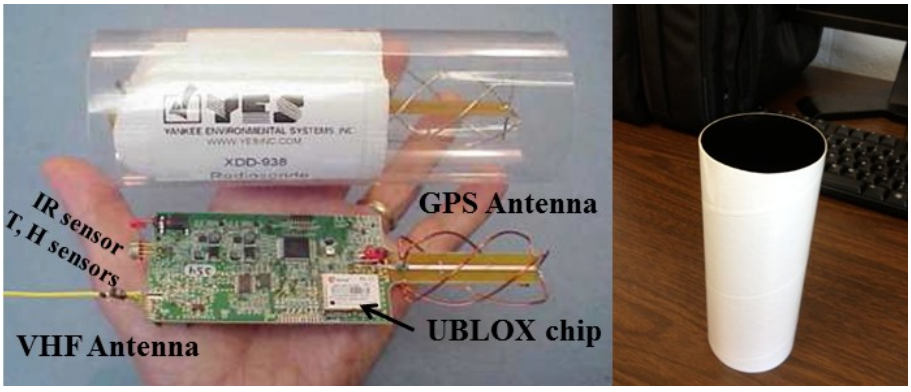

Figure 1. At left is the earlier XDD version used in the CIRPAS Twin-Otter experiment. Its outer sleeve was clear plastic showing the inner foam inner body within. The printed circuit board (PCB) is shown below, with uncoiled telemetry and GPS antennae and sensor locations. At right is today's XDD with biodegradeable cardboard cylinder coated black inside and white outside to minimize radiation effects, and are a revised electronic design. Weight is 58 g and size is 17.8 cm long by 6.6 cm in diameter.

The later XDD versions deployed by the WB-57 measured vertical profiles of PTU at 2-Hz, GPS-derived velocities at 4-Hz and Sea Surface Temperature (SST) at a 1 Hz. Longitude and Latitude and "housekeeping" data are reported at lower rates. (Earlier version XDDs used at CIRPAS reported all variables at 1 Hz.)

The configuration of HDSS evolved for each of the four aircraft installations discussed here as various components were developed and improved. For the Twin Otter installation, the HDSS v.1 prototype had a single dispenser with a 48-sonde magazine and one receiver. The system evolved

to HDSS *v.2* with both improvements to the XDDs and hardening of the dispenser for pressurized aircraft. Certification of *v.2* for flight in pressurized aircraft was awarded for the P-3 installation by NASA WFF (see S1-S3).

The moderate-altitude DC-8 deployments were done with manual release to demonstrate survival of the XDDs with high IAS deployment, and operation of forward error correction on two receivers to enable a long 160 km link range.

The *Mark-B* HDSS system flown on the WB-57 consists of two dispensers (S3). Dual paired dispensers allow launch rates faster than once every 5 seconds if needed, provide redundancy to enhance reliability and use available aircraft space better than a long single magazine. The Mark B dispensers have a magazine fore-body that holds 12 sondes on each side, with an optional magazine extender to accommodate 48 on each side. There was no need for the extenders on this flight given the number of sondes to be deployed and the paired units. Each dispenser has a full receiver and control-computer; this provides system redundancy. Both of the receivers in the dispensers were fed from a single antenna and pre-amp mounted on the underbelly of the WB-57 pallet. Each receiver can handle all the channel capacity, tracking up to 48 in flight simultaneously with error correcting telemetry.

The system demonstrated on the WB-57 also carried two additional receivers, one each for antennas mounted near the wingtips of the aircraft. The purpose of the two other receivers was to take advantage of antenna diversity; to allow signals to be received when the aircraft was turning when otherwise the wing and bank-angle would result in shadowing the belly antenna. The HDSS also carries two cameras to record dropsonde ejection: one aft of the drop-tubes facing forward, one forward of the drop-tubes facing aftward. These cameras also documented cloud structures ahead of and behind the aircraft. The mission monitor display for the WB-57, used to maintain situational awareness of XDD status in the dispensers as well as post-launch status and parameter display, is shown in S?. The configuration flown on the WB-57 weighs 104 kg.

Twin Otter HDSS/ XDD evaluation experiment

The first experiment used the NPS CIRPAS Twin Otter aircraft (S1) operating from Marina, CA. XDD data are compared with the instrumented research aircraft, Vaisala RD-94 dropsondes, and NDBC surface buoys. The locale provided nearby NDBC moored buoys, and an atmosphere with large changes in temperature and humidity across the top of the offshore marine layer in order to test instrument response in strong gradients. Twin Otter flights were conducted on 24 and 25 June, 2011, when only minimal low-level cloud cover was present at the top of the marine layer near the buoy locations as shown by GMS west visible satellite cloud images for overflight times on these two days shown in figure 2.

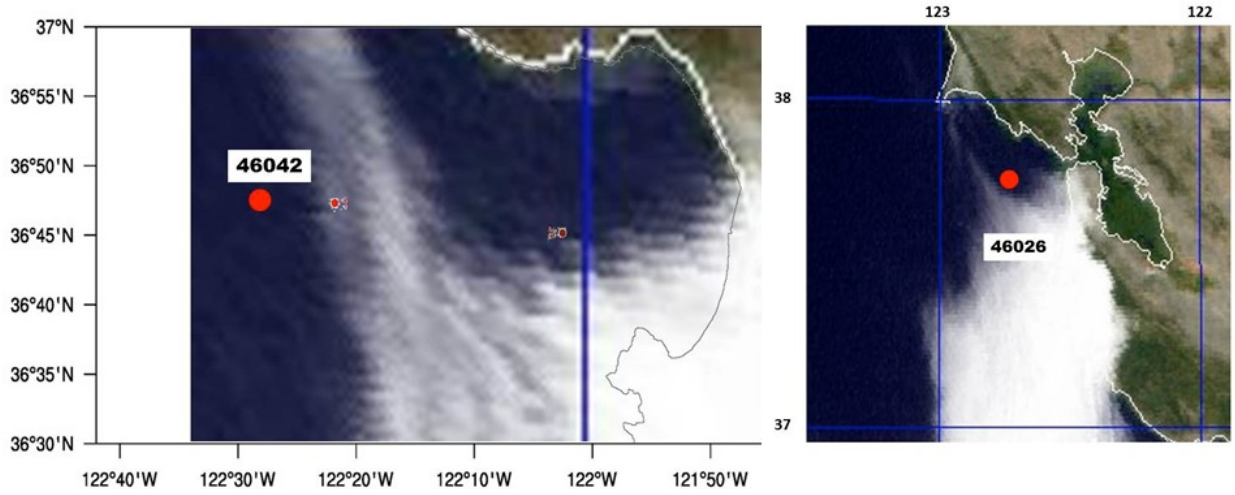

Figure 2. Visible satellite image showing stratus cloud cover and NDBC buoy 46042 location at the time of the Twin Otter dropsonde intercomparison flight on 24 June (left) and NDBC buoy 46026 location at the time of the Twin Otter dropsonde intercomparison flight on 25 June (right). Courtesy NRL satellite image archive: http://www.nrlmry.navy.mil/sat-bin/epac_westcoast.cgi

The Twin Otter standard meteorological instrumentation package (Jonsson, personal communication) was utilized with aircraft spiral descents/ascent at the same rate as the dropsonde fall rates to act as 'an impartial reference.' A standard NCAR Atmospheric Vertical Atmospheric Profiling System (AVAPS) system, part of the Twin Otter instrumentation suite, was used together with two deployment tubes, one designed to launch standard dropsondes and another for AXBT sonobuoy deployment. The latter was sleeved for the XDD dropsondes so that simultaneous deployment of RD-94 and XDD dropsondes was possible.

All analysis of RD-94 data was done on the "D-files." All analysis of XDD data was done on the data as telemetered directly by the detectors. The goal of this was to compare measurement to measurement. Telemetry errors for both systems were artificially low in these flights because the aircraft was never more than a few km away from the sondes during descent.

Two NDBC moored buoys were chosen as a second 'reference standard' for comparison of surface meteorological variables. The tests consisted of dual launches of the RD-94 and XDD sondes from 4 km altitude over NDBC buoy 46042 off Monterey Bay on the 24th and from 4 km altitude over NDBC buoy 46026 off San Francisco Bay on the 24th. The dual launches were followed immediately by the spiral descent of the aircraft at a rate close to that of the sondes. Sonde fall rates for the 25th are shown in S?. XDD slow-mode fall rates without a parachute are similar to RD-94 fall rates with a parachute.

Aircraft flight patterns were designed so that pairs of RD-94 and XDD sondes were deployed from 4 km altitude followed immediately by aircraft spiral descents to 60 m at approximately the fall rate of the sondes, which were nearly equal to each other, at 10-12 m/s. This was accomplished on both days followed by a slower ascent back to 4 km altitude with two-minute straight and level legs upwind and downwind at 6 levels during the ascent. This latter maneuver determined aircraft true airspeed and wind errors. Corrections were applied resulting in aircraft

winds independent of heading during spiral descents.

a. Comparison between XDD and RD-94 dropsondes and NDBC Buoy data

Figure 3 shows the three point weighted smoothed air temperature and humidity profiles for 24 June over buoy 46042 as a function of geopotential altitude (GA) for Vaisala (V) RD-94 sonde and YES (Y). A nine point smoother was used for pressure winds and SST. Figure 4 shows the data for the second flight on 25 June. XDD sondes indicate a small warm bias for XDD relative to RD-94 of 0.5–1.0°C throughout the profile with larger biases of 1-2°C in the upper levels between 3-4 km (seen best in the linear height plot on the left). Both sondes required about 15 s, or about 200 m vertically, to acclimate to the outside environmental temperature just after release from the aircraft. Slightly larger than average warm XDD biases relative to RD-94 were also observed within the marine layer, best seen in the right panel. Extrapolation to the 1-m elevation buoy air-temperature observation yields RD-94 air temperature about 0.5°C cooler than the buoy temperature of 11°C, with the XDD about 0.5°C warmer. The 20°C air temperature maximum at the top of the inversion and the 10°C minimum and the base of the inversion are well resolved by both sondes.

The RD-94 and XDD sondes also observed interesting wind features associated with the features described above in the temperature profile (figures 5, 6). The RD-94 and XDD wind speeds and directions are almost identical to each other with no significant differences. They observe interesting oscillations of the wind with height, most prominent of which are: 1) the upper level wind maximum (3.8 km) at the top of the upper inversion (3.5-3.7 km), 2) the strong wind shear below throughout the upper half of the adiabatic layer (3.5-2.6 km) down to the top of the very dry layer at 2.5 km, 3) the nearly constant wind with height layer throughout the dry layer (2.7-1.25 m), 4) followed by another strong wind shear layer to a wind minimum at the top of the marine inversion (1 km), 5) a third strong wind shear layer throughout the inversion, likely associated with a near-critical Richardson number of 0.8 (less than 1, but more than the critical value of 0.25) and associated Kelvin-Helmholtz instability, extending to a strong wind maximum (6) at the top of the marine layer. It is interesting to note that in the satellite images for both the 24th and 25th, wave-like features with a constant wavelength of 2.3 km can be observed in the stratus clouds, the constant wavelength being typical of Kelvin-Helmholtz instability as opposed to dispersive gravity waves. And finally, the sondes observe 7) frictional shear throughout the adiabatic marine layer following the log law to 35 m, below which a constant wind with height layer (8) is observed. Both RD-94 and XDD slow-sondes observe these features well.

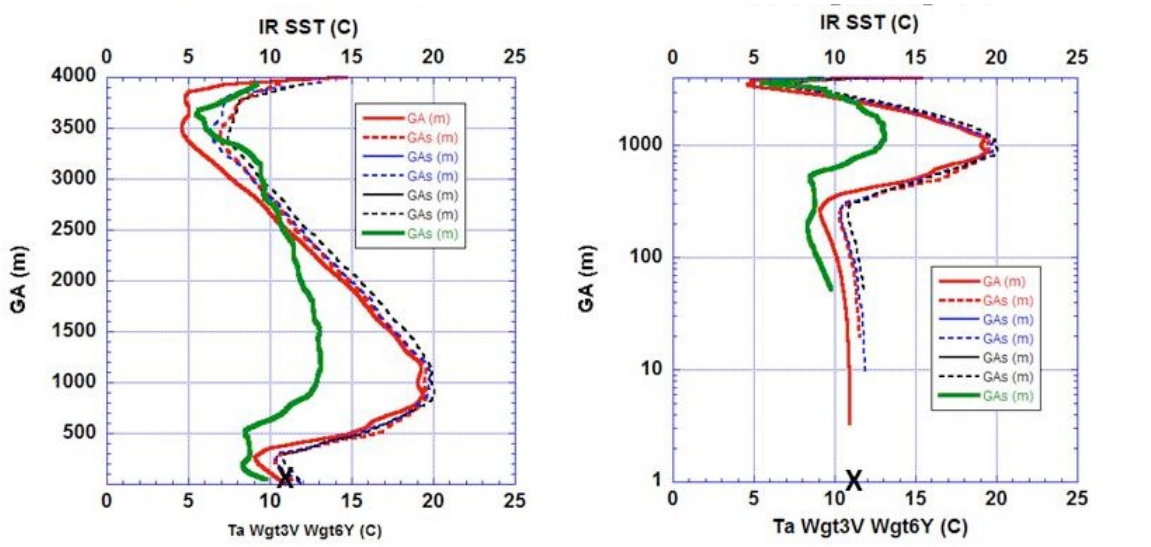

Figure 3. Comparison between YES XDD and Vaisala RD94 dropsonde profiles of air temperature, Ta, deployed from CIRPAS Twin Otter aircraft on 24 June 2011: linear geopotential height coordinates on the left, log coordinates, emphasizing boundary layer detail, on the right. Also shown is the XDD 'effective' SST profile as well as observed buoy SST at the surface. Vaisala Ta is in solid red , YES Ta is in dashed blue and black. XDD infrared-derived SST is plotted for comparison (solid green), X is SST from NDBC buoy 46042.

Corresponding to the wind speed features in Fig. 5, there is little directional shear of the wind within the upper wind maximum and the upper inversion layer (1). However, strong directional shear accompanies the wind speed shear within the upper adiabatic layer extending to the top of the dry layer at 2.5 km (2). Then, in contrast to the constant wind with height in the dry layer, the wind direction oscillates through two cycles of 30° direction changes reaching a minimum just at the top of the marine layer inversion. Strong direction shear accompanies the strong wind shear throughout the inversion extending to the wind max at the top of the marine adiabatic layer.

Within the marine layer the wind rotates cyclonically with height due to near-surface frictional effects. Therefore, not only are the observations repeatable and consistent between sonde types, the observations are also consistent with typical meteorological features observed above and below the marine layer off the coast of northern California.

The humidity sensor used in the XDDs at the CIRPAS intercomparison is slower than the sensor used in the RD-94s. Nonetheless comparison of humidity profiles in figure 3, 4 between RD-94 and XDD sondes show consistent features in the humidity measurements: 1) upper moist layer at the base of a temperature inversion (3-3.5 km, left panel),

2) dry, adiabatic layer from the top of the marine layer inversion (1.25 km) to the base of the upper moist layer 2.7 km), 3) strong moisture gradient from the top of the marine layer inversion to the top of the adiabatic marine layer (250 m) and 4) the cool, moist adiabatic marine layer at constant humidity (250m to the surface, right panel). The prime difference between the RD-94 and XDD humidity profiles is that the XDD profiles are about 5% wetter than the RD-94 in the upper levels (left panel) and about 10% drier within the marine layer below 500m (right panel); this latter difference is not explained by time-constants**.**

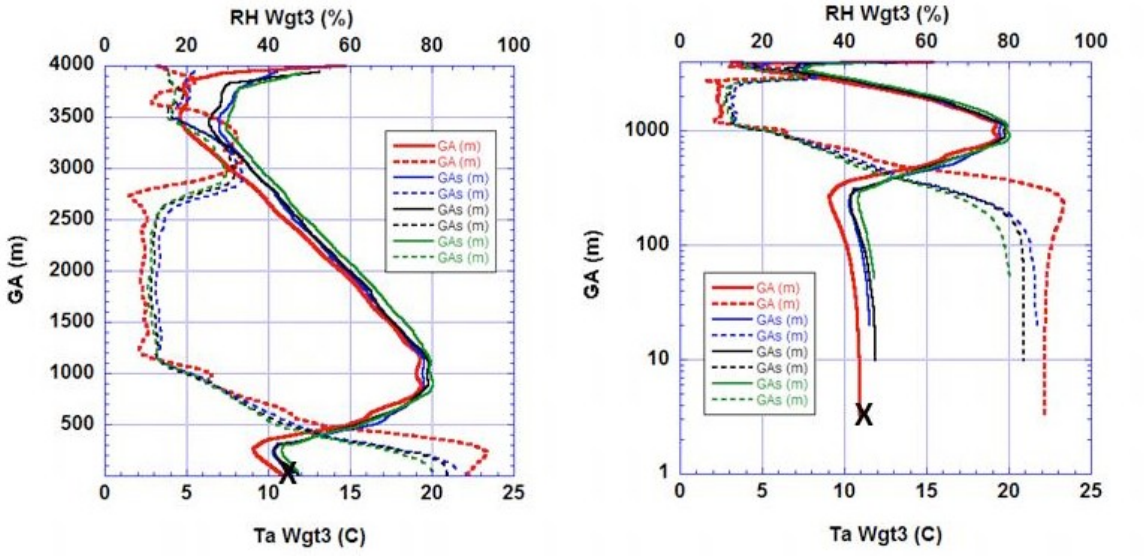

Figure 4. Comparison between YES XDD and Vaisala RD94 dropsonde observations from CIRPAS Twin Otter aircraft of Ta, air temperature (solid) and RH, relative humidity (dashed) during Flight 2, 25 June 2011vs a) linear geopotential height (left) and b) log geopotential height (right), designed to emphasize boundary layer detail. RD-94 data is in red, XDD data in blue, black and green. X is data from NDBC buoy 46026.

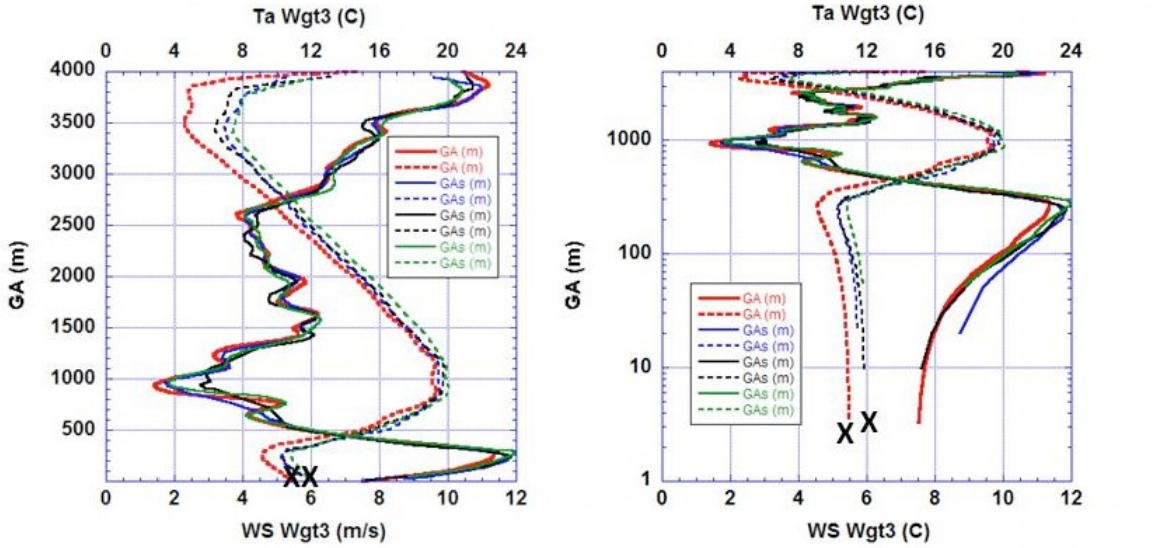

Figure 5. Comparison from CIRPAS Twin Otter aircraft between YES XDD and Vaisala RD94 dropsonde observations of wind speed (solid), WS and air temperature (dashed), Ta – Flight 2, 25 June 2011: linear geopotential height coordinates on the left, log coordinates, emphasizing boundary layer detail, on the right. Vaisala data is in red , YES data in Blue, black and green. X is data from NDBC buoy 46042.

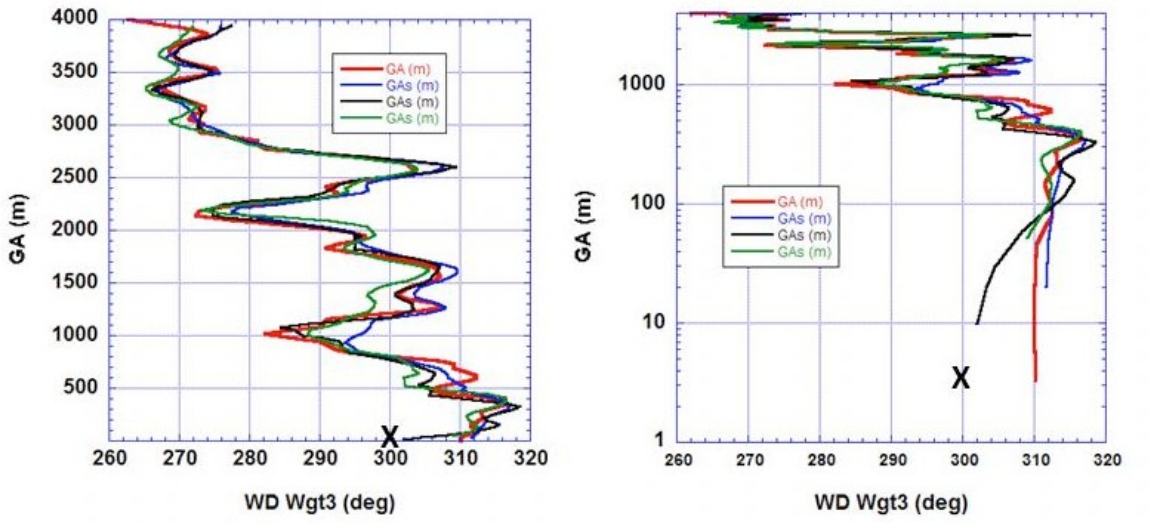

Figure 6. Comparison from CIRPAS Twin Otter aircraft between YES XDD and Vaisala RD94 dropsonde observations of wind direction WD– Flight 2, 25 June 2011: linear geopotential height coordinates on the left, log coordinates, emphasizing boundary layer detail, on the right. Vaisala data is in red, YES data in blue, black and green. X is data from NDBC buoy 46026.

The performance of the XDDs at the CIRPAS intercomparison was hindered by using the slow-mode to attempt to match fall-rates. Independent testing after the CIRPAS experiment made the impacts clear to us, which we show using data from the DC-8 flight. For this reason discussion of flight variances of slow-mode and fast-mode sondes are shown together later.

b. Comparison of XDD and Twin Otter SST observations

Figure 7 shows comparison profiles between XDD sondes and the Twin Otter wind speed (upper left), wind direction (upper right), air temperature (bottom left) and humidity (bottom right) profiles. Agreement is evident between both wind speed and wind direction profiles, with vertical spatial scales on the order of 500 m or less being well resolved.

The SST measurement provided by the XDD is obtained from an infrared detector in the 8-12 um 'water-vapor window' infrared band. This window is not entirely transparent to atmospheric water vapor and oxygen, the two main atmospheric emission sources in this band. The SST is simply taken from the lowest sonde reporting level, where column water vapor contributions are negligible. Flight profiles of the SST measurements are shown in S?.

DC-8 XDD observations

The DC-8 XDD deployments were a piggy-back mission on a NASA flight to monitor a satellite launch from Vandenberg AF Base, CA. The sonde deployments were made on the return leg from 12-21°N approximately along 119°W, directly along a dry air intrusion to the east of former Tropical Storm Cosme, as shown in figure 8. Three fast-fall sondes (magenta, pink and gray symbols) with sea-level fall speeds of 18 m/s were deployed from 0300-0330, 28 June, 2013 followed by 3 slow-fall sondes from 0330-0400 GMT, 28 June (blue, red and white symbols).

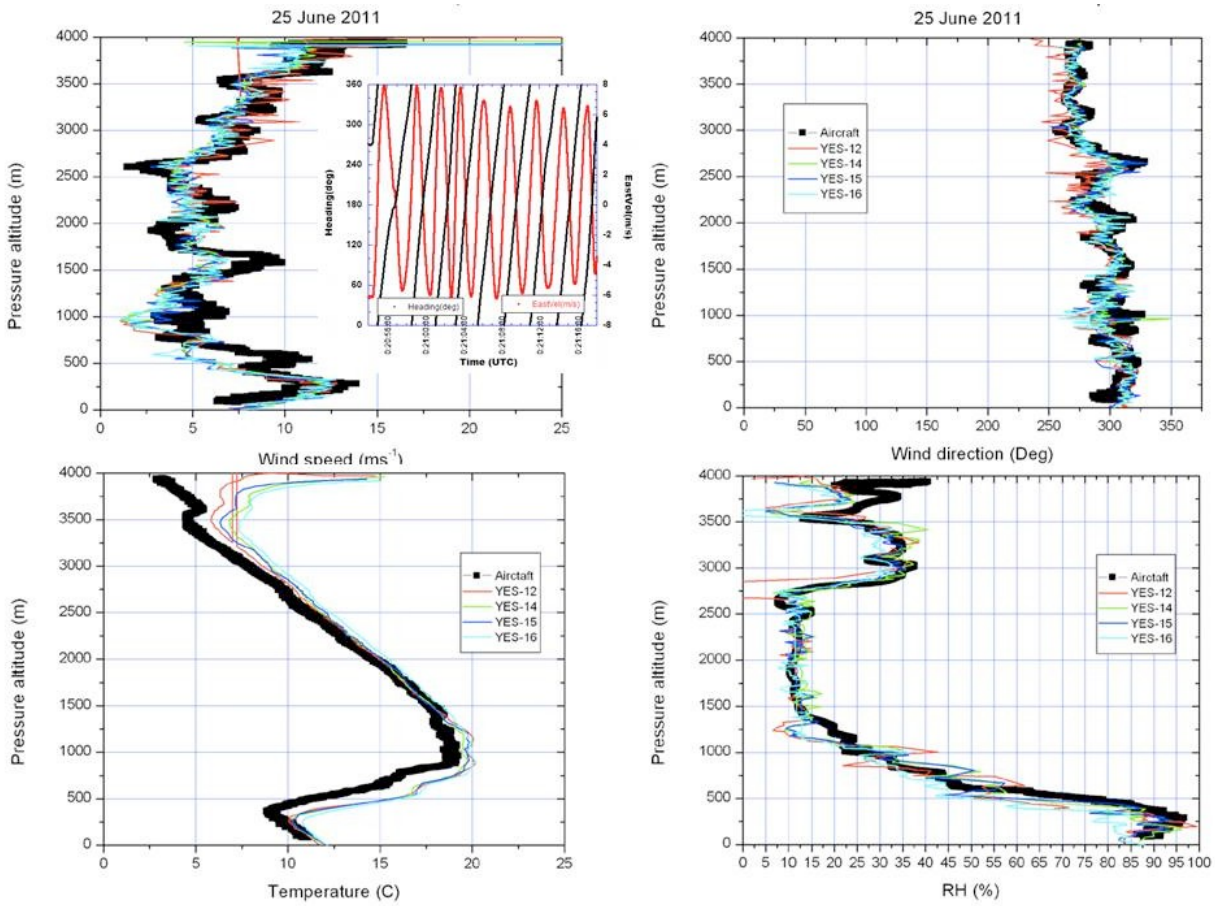

Figure 7. **Comparison of XDD sonde profiles with Twin Otter aircraft vertical profiles during spiral descent on 25 June over buoy 46026of a) wind speed (upper left), b) pressure (upper right), c) temperature (lower left) and d) relative humidity (lower right). Inset shows the the aircraft heading and east-west component of the wind as a function of time.**

The sonde locations relative to Cosme's center ranged from 1000 km SSE for the first sonde to 450 km ESE for the last sonde, was at the DC-8 point of closest approach to Cosme's center. Figure 8 also shows the location of three SST drifting buoys, one of which was located only 20 km from the last sonde drop. The SST pattern from a combined IR and microwave SST product is shown in S?[1] Ground truth estimates of SST from this product as well as from the drift buoy observations showed agreement with the sonde SST to within 0.5°C. S? provides estimates of surface winds from AMSU and ASCAT satellite sensors near 00 UTC, 25 June, about 3 hr prior

[1] Remote Sensing Systems, http://images.remss.com/hurricane/2013/sst/nep/

to the sonde deployments. These observations[2] indicate that surface winds along the DC-8 flight track were between 7-10 m/s.

Sonde trajectories are computed relative to the sonde location at the time of launch and shown in S? The fast-fall sondes traveled only 3.5 to 4.0 km to the north and northeast, consistent with upper SE winds shifting to lower SW winds. The slow-fall sondes however, travelled 9-12 km before splash; they travelled almost as far horizontally and they did vertically (13 km). This would be true of RD-94s under these conditions also. For slow-fall sondes care must be taken when interpreting profile parameters as vertical.

Compared with the fast-fall sondes, which lost less than 1% of observations, the slow-fall XDDs lost upwards of 20% of potential observations as a consequence of the varying transmit antenna orientation.

Inspection of the air temperature and SST in S? and the humidity in figure 9 show that sharp changes measured by these sensors in the vicinity of an inversion layer at 1.5 km (see right panels for detail) suggest adequate instrument response to resolve important small-scale atmospheric features. Of particular interest is the behavior of the SST for fast fall sonde #75-1. The measured infrared SST increases as it passes through the inversion, while all the other sondes transition to a constant SST *vs*. height across the inversion. This suggests that sonde #75-1 descended through a cloud layer measuring cold cloud top temperatures until it fell through the layer and again could see the surface. This behavior shows time response adequate to observe realistic features without acceleration. The decrease of humidity to near zero above 10 km is discussed below.

In Fig 10, the derived parameters of θ and θ_e show remarkable similarity from sonde-to-sonde with little difference between fast fall and slow fall. Similar small features seen in the θ_e profiles (right panel) especially suggest that realistic features are being resolved and that the measurements are repeatable. This conclusion is further enhanced in Fig 19 showing the wind speed and direction profiles. One can observe boundary layer double wind maxima, with vertical scales on the order of 200 m, above the top of a constant wind layer that are resolved by several sondes.

Flight Variances

The statistics of high-frequency variances are shown from the DC-8 flight in figure 12; data from three fast- or three slow-mode XDDs are combined in each histogram. The histograms of variance shown are the absolute value of the variance in the reported data passed through a 6-

[2] Courtesy Cooperative Institute for Research in the Atmosphere, Colorado State/NOAA, http://rammb.cira.colostate.edu/products/tc_realtime/storm.asp?storm_identifier=EP032013

point high-pass binomial filter[3], for the sounding data from 10 seconds after launch to an altitude 100 m above the boundary layer transition.

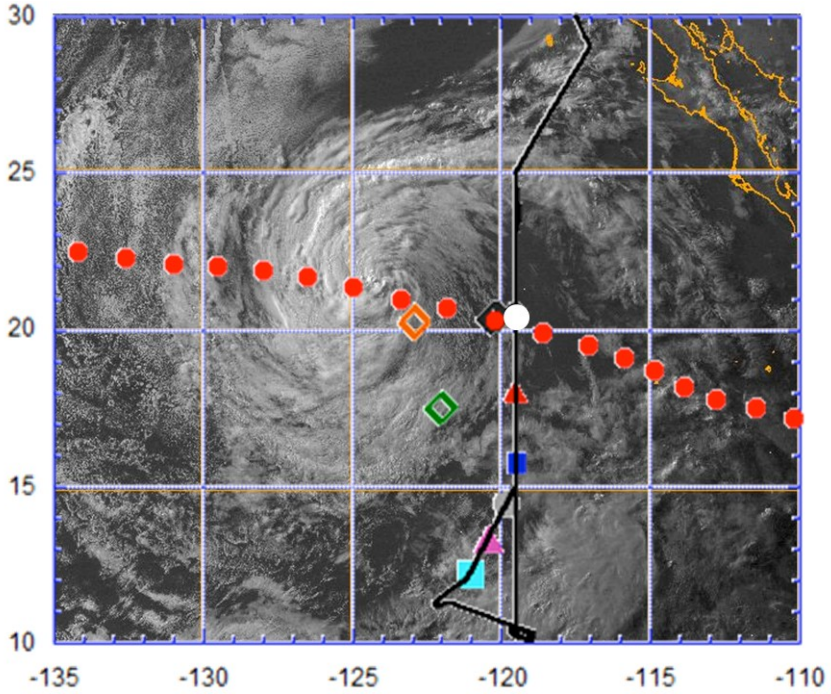

Figure 8. Visible GOES visible satellite image of Tropical Depression Cosme for 0130 UTC, 28 June. Cosme's NHC-derived Best Track 6-hourly positions from 1200 UTC, 25 June to 0000 UTC, 30 June are shown by the solid red circles. The NASA DC-8 flight track is in black with outbound and return legs overlapping north of 15N. During the return leg, three fast-fall eXpendable Digital Dropsondes (XDDs) were deployed along the diagonal flight leg from 13-15N, indicated by the sky-blue square, magenta triangle and grey circle from 0301-0321 UTC. These were followed by the deployment of three slow-fall XDDs indicated by the solid navy-blue square, red triangle and white circle from 0331-0407 UTC. In addition, the location of three SST drifting buoys are indicated by open black diamond (WMO #46911), open orange diamond (WMO #46910) and open green diamond (WMO #46916).

[3] The high-pass binomial filter is constructed by subtracting the original data from that which has been filtered by a six-point binomial FIR filter.

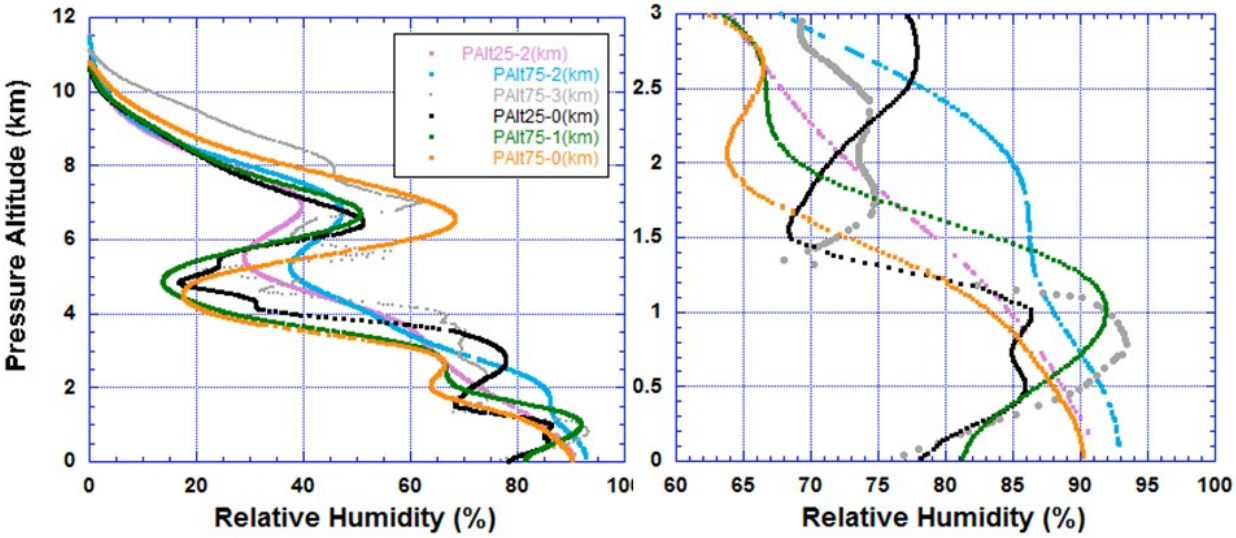

Figure 9. **Smoothed Relative Humidity (%) profiles for entire sounding (left) and air-sea boundary layer (right). Colors for slow- and fast-fall sondes are as in Fig. 10.**

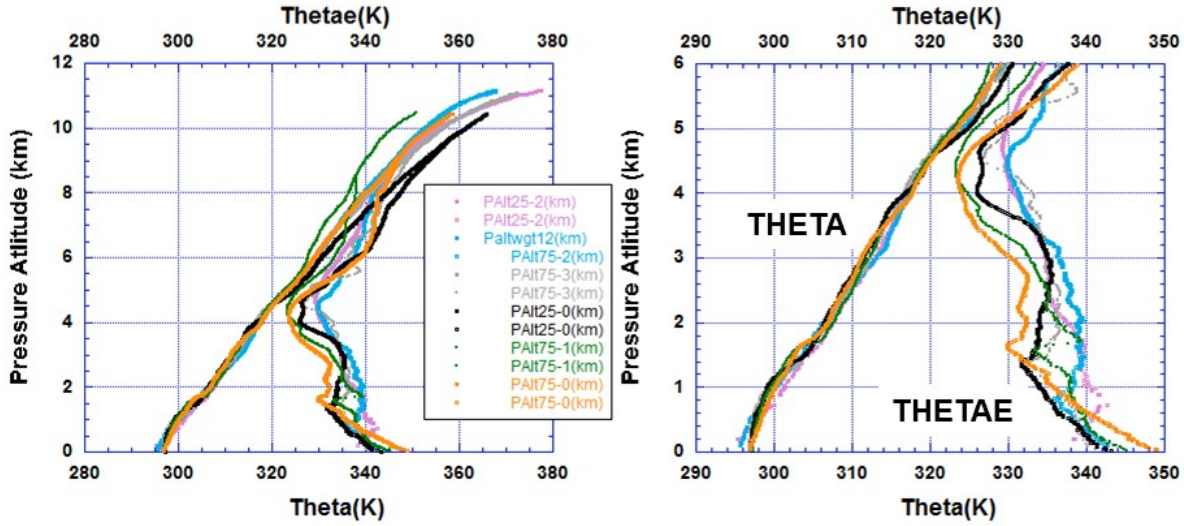

Figure 10. **Theta and Thetae (K) profiles for entire sounding (left) and mid- and lower-troposphere (right).**

For simplicity we identify this as the "flight variance:" clearly it is the combined effects of real profile variance, instrument noise, and the effects of perturbations in sonde velocity on the measurements.

These data show in hindsight that the choice to deploy only slow-mode sondes at CIRPAS as part of the intercomparison protocol in an attempt to match the descent rate of the parachute-equipped RD-94s (on the belief that this was critical to a "fair" intercomparison) was very harsh to the XDDs; the erratic spiral-dive and descent rate of the slow-mode aliases into all measured parameters. The horizontal winds are most affected, yet none of the measurements are improved. Seeing these results, it is remarkable how well the XDDs did in resolving the profiles as described.

For comparison the RD-94 data taken from CIRPAS effort are shown in these plots. Rigorously they are "apples to oranges," but they are the only co-located RD-94/XDD data we have. The slow-mode variances seen in the XDDs at CIRPAS are nearly identical to those from the DC-8 tests, differing in both RMS variance and mean(abs(variance)) by less than 20% with the slow-mode data shown here, for all parameters *except* temperature. The slow-mode temperature variance in the DC-8 soundings was almost twice that of the CIRPAS soundings; not surprising considering the meteorologies. We believe that some conclusions can be drawn, because the observed differences of the variances in several variables are large, and consistent with sonde physics. Small differences should not be interpreted as significant.

Due to apparent higher atmospheric variability of temperature in the DC-8 data the comparison of fast XDD (from DC-8) to RD-94 (from CIRPAS) yields inconclusive results. The thermistors are very similar, we expect their intrinsic responses to be similar. In the Reynold's number limit the heat flux scales as approximately ρV; the thermistor's measurement length constant will be nearly invariant with sonde fall-velocity if it is the velocity which ventilates the thermistor.

The RH variances cannot be taken at face value due to the differences in the detector time-constants; the RD-94's polymer sensor is faster and we expect it to respond to atmospheric variances to a greater degree, which cannot be understood without independent high-spatial-frequency data of the atmospheric humidity profile we do not have. However in all of these histograms the last bin contains all more-extreme outliers in the variance. We do not believe the population of outliers seen in the RD-94 humidity data is physically plausible even with faster frequency response; we have no explanation for these.

In contrast the GPS data presented here are identical GPS chipsets on both the RD-94s at CIRPAS, and the XDDs at CIRPAS and on the DC-8 flight. These data show a simple result: the fast-mode XDDs do not experience the parachute flutter and "pendulum dynamics" of the RD-94. The data they measure are thus less affected by variable drag force perturbations of their velocity. (Interacting as V * grad(S)) The wind and fall-speed data from fast XDDs show far less 1-Hz variance than the RD-94s.

A final point is the outliers in all graphs. The data show that the fast-mode XDDs do not exhibit outliers beyond the ranges shown, and neither do the RD-94s for any variable except RH. The slow-mode XDDs do show substantial outliers, which we are sure are not detector or telemetry "noise"; we conclude they are due to the erratic flight of the slow-mode descent sondes.

Drag coefficient of the fast sonde *vs.* Reynold's number is presented in S?, together with an argument that XDD fast sondes can measure vertical air motion much more accurately than existing RD-94 dropsondes that use a parachute.

XDD deployment from WB-57

The HDSS unmanned "Mark-B" system was tested on NASA's WB-57 operating from Ellington Field, Texas. During the period 13-19 November, 2013, three flights were conducted along a racetrack pattern from just offshore from Corpus Christi (CRP) to Brownsville, (BRO). Flights were approximately 2.5 hr each, spanning the time from 1100-1330 GMT, timed to

overlap early morning 1200Z NWS radiosonde ascents from CRP and BRO. The first two shakedown flights identified several integration problems on the new aircraft platform; improvised solutions allowed the third flight (the 19th) to be successful. In addition to establishing the Technology Readiness Level at 8, a number of operational experiments explored performance at high altitudes. Among these, Ku band satcom was operated continuously to explore potential XDD telemetry interference. No interference was found.

Planned (yellow) and actual (red) flight tracks for the third flight on 19 Nov are shown in figure 11, superimposed upon a BRO radar image and GOES IR satellite image using NASA's Mission Tool Suite (MTS) flight monitoring system. The latency on the weather radar was about 5 min, but closer to 1 hour for the satellite. For this reason the radar and IR cloud features do not align perfectly. Twenty three XDD dropsondes were successfully launched with no jams, and a series of eight deployed in less than one minute, as the WB-57 flew over the mini-squall line just east of the south end of the track, shown from the forward looking HDSS camera in S?. To verify safe fuselage separation during ejection the back seat observer monitored the HDSS' aft and forward-looking cameras. Camera imagery showed conclusively that each XDD fell away from the aircraft immediately, posing no threat to the aircraft. These cameras also proved extremely useful in enhancing situational awareness regarding flight progress relative to cloud features and rain areas for the science team on the ground via the Ku satcom link.

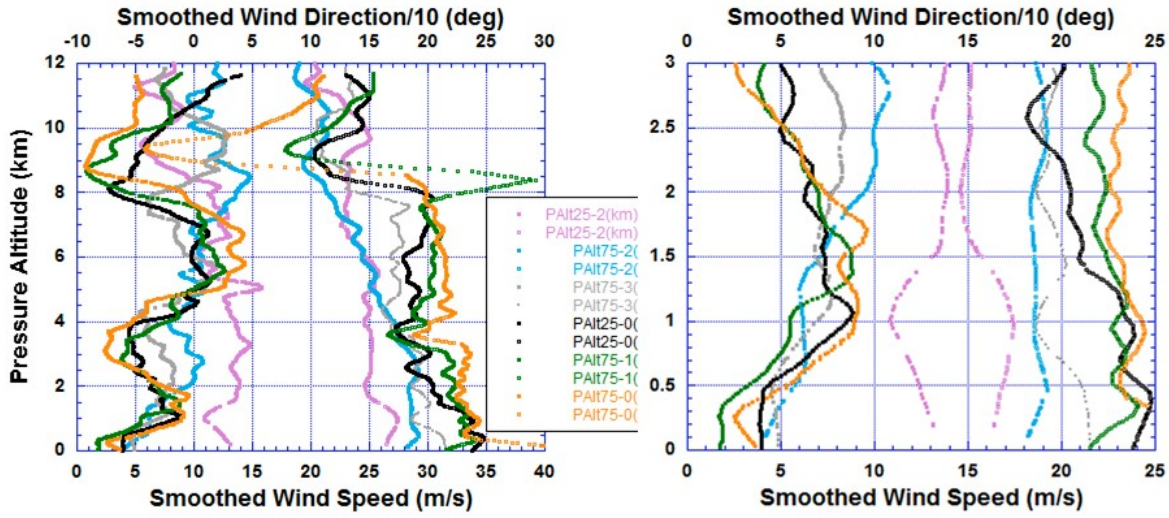

Figure 11. **Wind speed (m/s) and wind direction (divided by 10) profiles for entire sounding (left) and air-sea boundary layer (right). Colors for slow- and fast-fall sondes are as in Fig. 9. Wind speeds are on left side of each panel and wind direction (divided by 10) on right side of panel.**

In addition to the first availability of the WB-57 on the MTS, the ground science team was able to monitor aircraft track, weather system evolution and HDSS function during the aircraft flight via a web-based interface. This display (S?) shows the status of XDD dropsondes not yet released in each of the two redundant ADDs, telemetry status of deployed XDDs, trajectory/PTU

data plots, views from forward/aft cameras, status of the Ku-band communication link, and an iChat window for text communication between the mission scientist and the on- board WB-57 mission manager.

Fig. 12 shows excellent agreement between the two XDD's and corresponding NWS radiosonde-derived wind profiles. These profiles illustrate the vertical structure of a subtropical jet with different structures at CRP and BRO. This upper-level feature was just behind a cold front that had passed off the Texas coast the day before the flight. Of particular interest is the capability shown by this plot that the XDDs resolve all the fine scale detail measured by the radiosondes including fluctuations on the scale of 200-300m. Both the XDD and CRP radiosonde observed a low-level wind maximum (from the northeast) at the north end of the WB-57 racetrack, consistent with its position further behind the cold front and more well-established northeasterly flow.

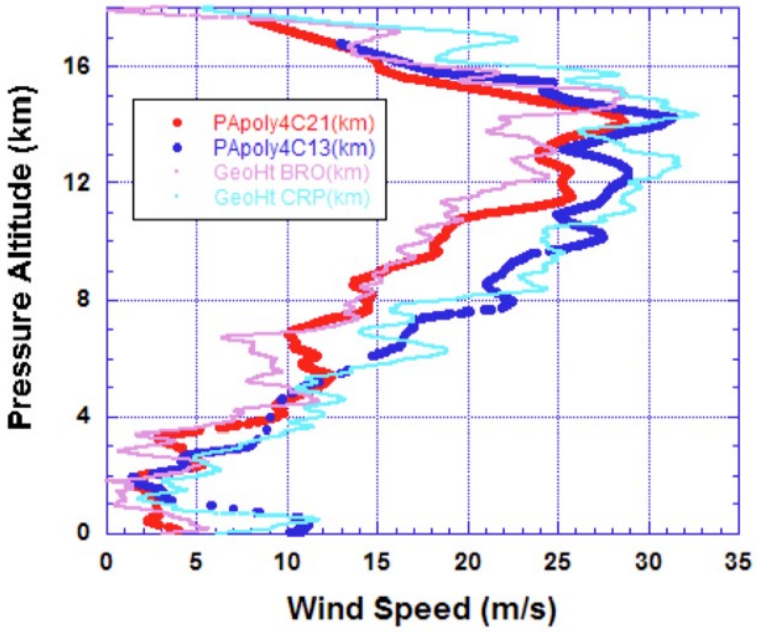

Figure 12. Comparison of wind speeds from slow-fall sonde, C13 (dark blue) located due east of Corpus Christi (CRP) and fast-fall sonde C21 (red) located due east of Brownsville (BRO) with radiosonde wind speed profiles from CRP (light blue) and BRO (magenta).

Fig. 13 illustrates the comparison of the temperature and humidity profiles observed from XDD dropsonde "C21" and the BRO radiosonde, which was excellent. The C21 upper level temperatures from 13-16 km are warmer than the radiosonde by about 10°C. We believe this difference is real as the XDD was dropped through the trailing edge of the thunderstorm anvil from the cells just east of the WB-57 drop point. The humidities near the surface observed by the BRO radiosonde over land are almost 100%, about 15% higher than observed by the XDD over the ocean. This again appears real as fog was reported at BRO at the time of the radiosonde launch; there was no fog over the ocean. The moisture maxima at 1 km, 3km, 5-6 km are well resolved by the XDD.

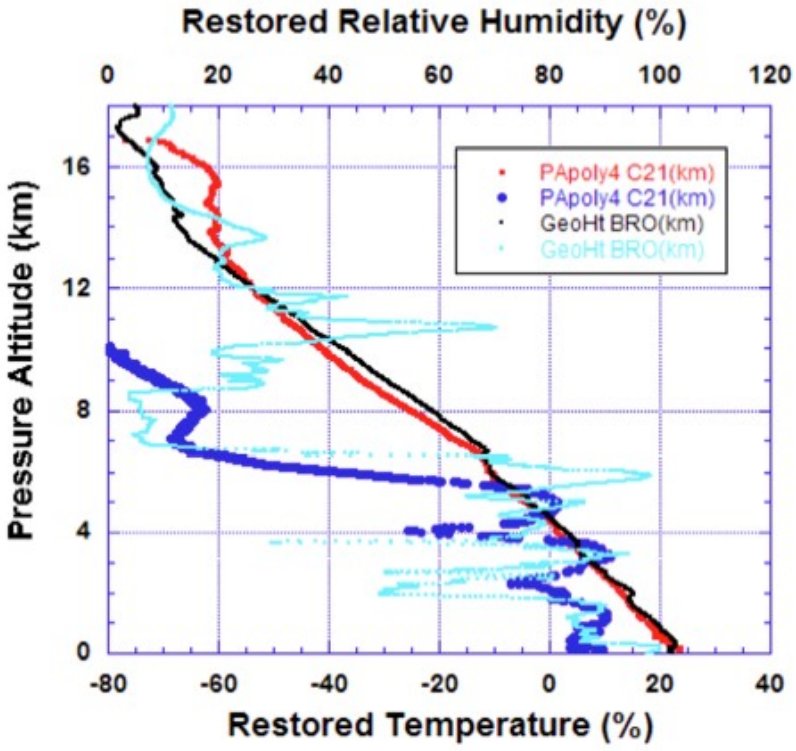

Figure 13. **Temperature and humidity profile observed by sonde C21 (red and dark blue, respectively) located east of BRO with the BRO temperature and humidity (black and light blue, respectively).**

Humidity at High Altitudes

The WB-57 flights were the first XDD deployments above 10 km and by design they do not report RH below -40°C; comparisons show that observed relative humidity is not reasonable at temperatures below -30°C. Upper air measurements by balloon-borne sondes have been a very difficult issue that is well covered in the literature, and it is made considerably more difficult from a dropsonde due to the relatively faster transit times and larger disequilibration at launch.

Similar behavior was noted by Revercomb, et al. (2013) showing the difference between AVAPS dropsonde relative humidities (deployed by Global Hawk) and S-HIS humidities using ECMWF model fields as a first guess in profile retrievals. They showed a consistent dry bias of 40% above 400 mb between AVAPS and S-HIS for 14 intercomparisons for 2012.

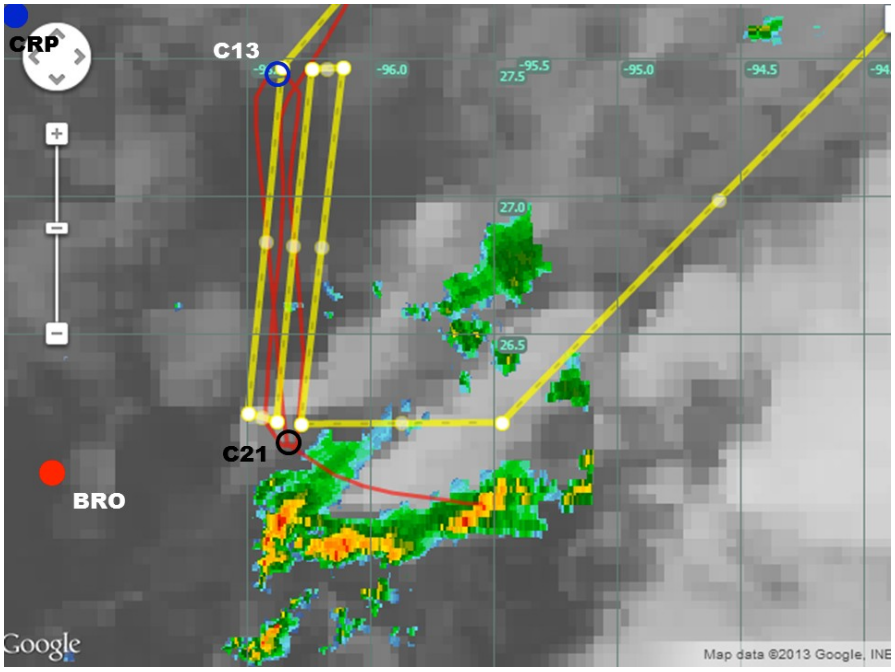

Figure 14. WB-57 test flight track planned (yellow) and actual (red) as flown on 19 Nov, 2013. The location of the Brownsville (BRO) and Corpus Christi (CRP) radiosonde stations are shown in red and blue, respectively. The locations are also shown of the two sample XDDs, the slow-fall sonde, C13 deployed off shore from CRP, and the fast-fall sonde, C21 deployed off shore from BRO. BRO radar display is overlaid on GOES geostationary satellite IR image

Summary and Conclusions

In this paper we describe the first field tests of the automated HDSS/XDD system developed to obtain more synoptic sampling of "high impact" weather systems with better spatial resolution. The HDSS system is the first autonomous drop-sonde system suitable for both pressurized and unpressurized aircraft. The XDD sondes deliver an accurate measurement of the sea-surface "skin temperature:" a new measurement for radiosondes.

We have shown that this new system has the capability for atmospheric profile measurements comparable to the widely-used Vaisala RD-94 unit; fast-mode XDDs have better resolution for winds and vertical velocities, similar performance for pressure and temperature, lesser resolution for RH profile.

Comparison of the mean XDD profiles with the RD-94 and Twin Otter spiral descent observations showed that the XDD's were warmer by about 1°C and drier by about 5% than the RD-94 and Twin Otter values. The twin Otter winds had to be heavily filtered due to oscillation associated with continuous heading changes during descent. However, the XDD and RD-94 winds were virtually identical during even small-scale fluctuations in the vertical. The winds measured by the aircraft were also in good agreement although small scale fluctuations could not be resolved due to the necessary filtering.

Two separate of cases (and buoys) showed that the mini-radiometer measured skin SST to within 0.5°C of *in-situ* moored buoy bulk SST at 1-m depth. Two XDD sondes floated on the surface

for tens of seconds and report temperature observations matched mini-radiometer SST values comparably.

During the DC-8 XDD test flight conducted in the Eastern Tropical Pacific just east of decaying Tropical Storm Cosme and west of the Baja Penninsula, a total of 6 sondes were deployed: 3 in spiral dive mode (slow-fall) and 3 in ballistic mode (fast-fall). The slow-mode exhibited larger 'flight noise' amplitudes and greater numbers of data drop-outs than did the fast ballistic mode, especially in the fall velocity and horizontal winds. We expect that most future deployments will use XDDs built for "fast mode."

The WB-57 campaign demonstrated the HDSS system from high-altitude, operating autonomously, and dropping XDD sondes into a precipitating convective storm.

To date the development effort for the XDDs has been driven by the goals of developing a capability to launch sondes at much higher rates, so that sampling densities can be improved, and demonstrating the improvements in system reliability and data returned so that more-extensive observations are feasible. We believe substantial progress on these goals is demonstrated: we acknowledge further improvement is desirable in several areas.

NASA has embarked on a program of refurbishment and modernization of the WB-57 and ER-2, making them valuable platforms for high altitude testing of various new technologies as well as development of atmospheric observational capability from the new generation of High Altitude Long endurance (HALE) Unmanned Aerial Vehicles (UAVs), such as the Global Hawk. HDSS offers the potential to extend existing profiling strategies, combining new deployment schemes with these aircraft. While the impact of dropsonde observations has been shown to improve TC track forecast by 20% (Burpee, et al., 1996), the e-folding time of this impact is estimated to be about 12 hours (Aberson, 2010). Use of NOAA GIV flights for 12-hourly repeat observations has been shown to provide additional improvement in TC forecasting by allowing for daily time changes in initial conditions to be more accurately resolved (Aberson, 2010). The use of the Global Hawk UAV provides for the potential of 24-hour duration flights and the deployment of dropsondes on a continuous basis. Improvements to COAMPS-TC forecasts using this new observational strategy in Nadine from 2012 has been suggested (Doyle, et al., 2014).

The HDSS offers improvements to airborne atmospheric profiling at a time of improvements in TC aircraft observing capability, even as TC satellite observing capability is declining (Hawkins, et al, 2013). Air Force Reserve Command (AFRC) WC-130J and NOAA WP-3D aircraft, used in operational hurricane reconnaissance missions for the National Hurricane Center (NHC), utilize surface wind sensing capability via the Stepped Frequency Microwave Radiometer (SFMR), technological improvements to existing dropsonde profiling, and use of operational airborne Doppler radar from NOAA G-IV and WP-3D aircraft all contribute new capability for TC numerical and statistic intensity prediction models. HDSS data can bridge the gap between 3-D Doppler sampling of winds only and the widely-spaced measurements of PTU and winds provided by existing dropsonde sampling strategies. It also adds IR remote sensing of SST.

Future Directions

Additional improvements to the HDSS system and XDD dropsonde are planned that will further enhance the capability of this system. From the work here one can see that improved time-

response would be desirable, particularly by comparison with the RD-94 and NCAR minisonde. This is a goal and we believe improvement can be made, but we do not expect that we could match these sondes at RH resolution without copying features of their design that degrade performance goals for the XDDs. Thus we expect these two systems will have overlapping but complementary strengths. The XDDs deliver better resolution of horizontal winds and we plan to demonstrate accurate air-motion vertical-velocity measurements. The goals for short-term XDD improvements are further improvements to telemetry and operational capability to enable much higher spatial density sounding data. To be useful this demands substantially better operational reliability and telemetry performance than has been the norm for dropsondes.

Additional flights are planned for 2014 as part of the ONR-sponsored Tropical Cyclone Intensity (TCI) experiment, for 2015 in collaboration with TCI and NOAA's UAV demonstration project: Sensing Hazards with Operational Unmanned Technology (SHOUT) and for 2016-17 in collaboration with TCI and, pending favorable project funding, NASA's OUTFLOW experiment, planned for the Western Pacific. The latter also depends upon support for HDSS integration on one of the NASA Global Hawks.

1. Acknowledgements

The authors gratefully acknowledge the support of the Office of Naval Research for providing Twin Otter and WB-57 flight hour support and manpower support for P. Black and R. E. Lee under contract numbers N00014010-C-028. Mark Beaubien and Yankee Environmental Systems, Inc. were supported through SBIR award N08-145. We express our thanks to Robert E. Lee, CMSgt Ret., for his assistance in the Twin Otter mission planning, equipment installation and resourceful sonde deployment, without whose help the project would not have been a success. The authors wish to thank the technical staff at CIRPAS, especially Roy Woods, as well as the Twin Otter pilots who flew the two missions. Without their help in system integration and flight planning, these flights would have been impossible. We thank the CIRPAS staff for providing assistance in tracking and monitoring the flights in real time and for processing the Twin Otter flight level data. We would like to thank the Air Force Reserve, 53rd.

Weather Squadron NOAA Aircraft Operations Center for providing consultation on integration of AVAPS system on the Twin Otter. Sincere appreciation is also extended to NASA Ames, Dryden Research Center and Johnson Space Center, WB-57 Program Operations. We are especially thankful to NASA Ames and DRC for permission to fly piggy-back on the flight over the East Pacific. Special thanks is extended to the WB-57 program managers James Alexander and Tim Propp, WB-57 flight crew and the entire engineering and IT staff of the NASA WB-57 Program Office. We also wish to thank Patrick Finch and Aaron Duley, NASA Ames, for last minute help in arranging for display of WB-57 flight track on the NASA Mission Tools Suite, greatly improving situational awareness. Thanks is also extended to NWS Brownsville Meteorologist-In-Charge, Steve Drillette, and Jim Campbell as well as NWS Corpus Christi personnel Lara Keys and Ian Blaylock for providing radiosonde data.

2. References

Aberson, S. D., and J. L. Franklin, 1999: Impact on hurricane track and intensity forecasts of GPS dropwindsonde observations from the first-season flights of the NOAA Gulfstream-IV jet aircraft. *Bull. Amer. Meteor. Soc*., **80**, 421-427.

Aberson, S. D., 2010: 10 Years of Hurricane Synoptic Surveillance (1997–2006). *Mon. Wea. Rev.,***138**, 1536-1549

Aberson, S. D., 2011: The Impact of Dropwindsonde Data from the THORPEX Pacific Area Regional Campaign and the NOAA Hurricane Field Program on Tropical Cyclone Forecasts in the Global Forecast System. *Mon. Wea. Rev.,***139**, 2689-2703

Ancell, B., G. J. Hakim, 2007: Comparing Adjoint- and ensemble-sensitivity analysis with applications to observation targeting. *Mon. Wea. Rev*.,**135**, 4117–4134.

Bender, M. A., I. Ginis, R. Tuleya, B. Thomas and T. Marchok, 2007: The Operational GFDL

Coupled Hurricane–Ocean Prediction System and a Summary of Its Performance. *Mon. Wea. Rev.*,**135,** 3965-3989

Black, P. G., E. D'Asaro, W. Drennan and J. R. French, P.P. Niiler, T. B. Sanford, E. J. Terrill, E. J. Walsh and J. Zhang, 2007: Air-Sea Exchange in Hurricane Winds: Synthesis of Observations from the Coupled Boundary Layer Air-Sea Transfer Experiment. *Bull. Amer. Meteorol. Soc*., **88**, 357-374.

Black, P. G., 2012: Tropical Cyclone Unusual Intensity and Structure Change in the Western North Pacific Observed by Reconnaissance Aircraft During TPARC/TCS08 and ITOP/TCS10**,** *J. Tropical Cyclone Res. and Rev.*, **1**, 75-88.

Burpee, R. W., S. D. Aberson, J. L. Franklin, S. J. Lord, R. E. Tuleya, 1996: The Impact of Omega Dropwindsondes on Operational Hurricane Track Forecast Models. *Bull. Amer. Meteor. Soc.,* **77**, 925-933

Chou, K-H., C-C. Wu, P-H. Lin, S. D. Aberson, M. Weissmann, F. Harnisch, T. Nakazawa, 2011: The Impact of Dropwindsonde Observations on Typhoon Track Forecasts in DOTSTAR and T-PARC. *Mon. Wea. Rev.,* **139,** 1728-1743

DeMaria, M., and J. Kaplan, 1999: An updated statistical hurricane intensity prediction scheme (SHIPS) for the Atlantic and eastern north Pacific basins. *Wea. Forecasting,* **14**, 326-337.

DeMaria, M., M. Mainelli, L.K. Shay, J.A. Knaff and J. Kaplan, 2005: Further Improvements in the Statistical Hurricane Intensity Prediction Scheme (SHIPS). *Wea. Forecasting,* **20**, 531-543. DeMaria, M., 2009: A simplified dynamical system for tropical cyclone intensity prediction. *Mon. Wea. Rev.,* 137, 68-82.

DeMaria, M., 2010: Tropical cyclone intensity change predictability estimates using a statistical-dynamical model. Extended Abstract, AMS 29th Conference on Hurricanes and Tropical Meteorology, May 10-14, 2010, Tucson, AZ. https://ams.confex.com/ams/29Hurricanes/techprogram/paper_167916.htm

DeMaria, M., C. R. Sampson, J. A. Knaff and K. D. Musgrave, 2014: Is Tropical Cyclone Intensity Guidance Improving? *Bull. Amer. Meteor. Soc.,* **14**, early release.

Doyle, J.D., C.A. Reynolds, C. Amerault, 2011: Diagnosing tropical cyclone sensitivity. *Computing in Science and Engineering*, **13**, 31-39.

Doyle, J. D., J. Moskaitus, P. Black, E. Hendricks and P. A. Reinecke, 2014: Upper level outflow, predictability and HS3 observational impact. AMS 31st Conference on Hurricanes and Tropical Meteorology, San Diego, CA, 31 Mar- 4 Apr, 2014.

Franklin, J. L., M. L. Black, and K. Valde, 2003: GPS dropwindsonde wind profiles in hurricanes and their operational implications. *Wea. Forecasting*, **18**, 32-44.

Gall, J. S., I. Ginis, S-J. Lin, T. P. Marchok and J-H. Chen, 2011: Experimental Tropical Cyclone Prediction Using the GFDL 25-km-Resolution Global Atmospheric Model. *Wea. and Forecasting,* **26**, 1008-1019

Gasiewski, A., A. Chaturvedi, E. McIntyre, D. M. Kraft, P. O. G. Persson, M. Tjernstrom, M. Beaubien and W. Jeffries, 2009: Use of a new generation of dropsondes during the 2008 Arctic Mechanisms for the Interaction of the Surface and Atmosphere (AMISA) campaign. 10th Conf. on Polar Meteor. And Oceanography, 18-21 May, 2009, Madison, WI https://ams.confex.com/ams/10POLAR/webprogram/Paper152908.html

Hawkins, J., T. Lee, K. Richardson, M. Surratt, C. Sampson, and J. Kent, 2013: The history of tropical cyclone remote sensing via satellite microwave imagers, AMS 94th Annual Meeting, History Symposium, Austin, TX, 6-10 Jan, 2013. https://ams.confex.com/ams/93Annual/webprogram/Paper223439.html

Hendricks, Eric A., Melinda S. Peng, Xuyang Ge, Tim Li, 2011: Performance of a Dynamic Initialization Scheme in the Coupled Ocean-Atmosphere Mesoscale Prediction System for Tropical Cyclones (COAMPS-TC). *Wea. Forecasting*, **26**, 650-663.

Hock, T. F., and J. L. Franklin, 1999: The NCAR GPS dropwindsonde. *Bull. Amer. Meteor. Soc*., **80**, 407-420.

Jin, H., M. S. Peng, Y. Jin and J. D. Doyle, 2014: An Evaluation of the Impact of Horizontal Resolution on Tropical Cyclone Predictions using COAMPS-TC. *Wea. and Forecasting,* early release

Jones, T. A., D. J. Cecil, and M. DeMaria, 2006: Passive Microwave-Enhanced Statistical Hurricane Intensity Prediction Scheme. *Wea. and Forecasting,* **21**, 613-635.

Kaplan, J., M. DeMaria, and J.A. Knaff, 2010: A Revised Tropical Cyclone Rapid Intensification Index for the Atlantic and Eastern North Pacific Basins. *Wea. and Forecasting,* **25**, 220-241.

Kepert, J. D., 2006: Observed Boundary Layer Wind Structure and Balance in the Hurricane Core. Part I: Hurricane Georges. *J. Atmos. Sci*., **63**, 2169-2193.

Knaff, J.A., C.R. Sampson, and M. DeMaria, 2005: An Operational Statistical Typhoon Intensity Prediction Scheme for the Western North Pacific. *Wea. Forecasting,* **20**, 688-699.

Miloshevich, L. M., H. Vömel, A. Paukkunen, A. J. Heymsfield, and S. J. Oltmans, 2001: Characterization and correction of relative humidity measurements from Vaisala RS80-A radiosondes at cold temperatures. *J. Atmos. Oceanic Tech.*,**18**, 135–156.

Persson, P. O. G., 2010: Summary of meteorological conditions during the Arctic Mechanisms for the Interaction of the Surface and Atmosphere (AMISA) intensive observation periods. NOAA Tech. Memo PSD-314, NOAA-OAR-ESRL, Boulder, CO, 57pp.

Rivercombe, H., J. Taylor, F. Best, D. Tobin, R. Knuteson, W. Smith, E. Weisz, D. Deslover, R. Garcia, D. Hoese and P. Antonelli, 2013: Scanning HIS: Advance IR Sounder for HS3. HS3. Science Team meeting, NASA Ames Research Center, 7-8 May, 2013. https://espo.nasa.gov/missions/hs3/content/HS3_Science_Presentations

Tallapragada, V., C. Kieu, Y. Kwon, S. Trahan, Q-F. Liu, Z. Zhang and I-H. Kwon, 2014: Evaluation of Storm Structure from the Operational HWRF Model during 2012 Implementation. *Mon. Wea. Rev.,* early release

Verver, GÉ, M. Fujiwara, P. Dolmans, C. Becker, P.L Fortuin L. Milosevitch, (2006) Performance of the Vaisala RS80A/H and RS90 Humicap Sensors and the Meteolabor "Snow White" Chilled-Mirror Hygrometer in Paramaribo, Suriname *J. Atmos. Oceanic Tech.,* **23**, 1506–1517.

Vomel,H., H. Selkirk, L. Milosevitch, J. Valverde-Canossa, J. Valdes, E. Kyro,& R. Kivi, W. Stolz, G. Peng, J. A. Diaz, (2006) Radiation Dry Bias of the Vaisala RS92 Humidity Sensor, J. *Atmos. Ocean Tech*. 24: 953 – 963 http://journals.ametsoc.org/doi/pdf/10.1175/JTECH2019.1

Weissmann, M., F. Harnisch, C-C. Wu, P-H. Lin, Y. Ohta, K. Yamashita, Y-H. Kim, E-H. Jeon, T. Nakazawa and S. D. Aberson, 2011: The Influence of Assimilating Dropsonde Data on Typhoon Track and Midlatitude Forecasts. *Mon. Wea. Rev.,* **139,** 908-920

Weng, Y-H. and F-Q. Zhang, 2012: Assimilating Airborne Doppler Radar Observations with an Ensemble Kalman Filter for Convection-Permitting Hurricane Initialization and Prediction: Katrina (2005). *Mon. Wea. Rev.,* **140**, 841-859

Wu, C-C., K-H. Chou, P-H. Lin, S. D. Aberson, M. S. Peng and T. Nakazawa, 2007: The Impact of Dropwindsonde Data on Typhoon Track Forecasts in DOTSTAR. *Wea. and Forecasting,* **22**, 1157-1176